

Acid-Modulated Synthesis of High Surface Area Amine-Functionalized MIL-101(Cr) Nanoparticles for CO₂ Separations

Gang Han, Katherine Mizrahi Rodriguez, Qihui Qian, and Zachary P. Smith*



Cite This: <https://dx.doi.org/10.1021/acs.iecr.0c03456>



Read Online

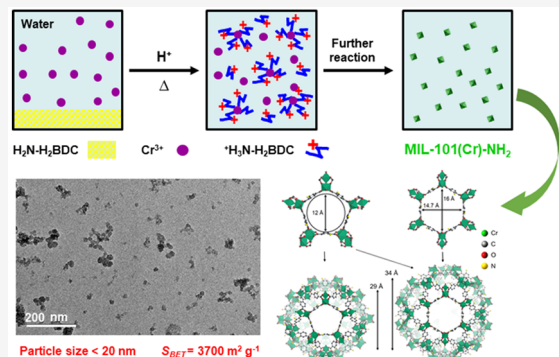
ACCESS |

Metrics & More

Article Recommendations

Supporting Information

ABSTRACT: Metal–organic frameworks (MOFs) have been gaining significant interest for separations involving CO₂. In this study, amine-functionalized MIL-101(Cr) (i.e., MIL-101(Cr)-NH₂) MOFs with sub-20 nm particle size and an ultrahigh Brunauer–Emmett–Teller surface area of $3700 \pm 200 \text{ m}^2/\text{g}$ were directly synthesized from 2-aminoterephthalic acid in water with the aid of acidic modulators. Acidic modulators are shown to yield significant changes in nuclei formation and crystal growth during MOF particle synthesis by enhancing the solubility of the 2-aminoterephthalic acid ligand in aqueous media through protonation of the amine groups while slightly suppressing the deprotonation of carboxylic acids. Owing to the ultrahigh surface area and Lewis basic amine chemistry, superior CO₂ uptake of 5.4 mmol/g was obtained by the synthesized MIL-101(Cr)-NH₂ at 1 bar and 278 K, which surpasses other MIL-101(Cr) MOFs reported to date. In addition, MIL-101(Cr)-NH₂ exhibits significantly higher CO₂/N₂ selectivities than the parent MIL-101(Cr) benchmark for an idealized flue gas mixture composed of 0.15 bar CO₂ and 0.85 bar N₂, as determined using ideal adsorbed solution theory at 323 K. The high CO₂ uptake and CO₂/N₂ selectivity are attributed to the high isosteric heat of CO₂ adsorption, calculated to be -59.5 kJ/mol at zero coverage. The successful preparation of high surface area amine-functionalized MIL-101(Cr) nanoparticles provides a great platform for further exploring the functionalities and applications of MIL-101(Cr)-based adsorbents and membranes for CO₂ separations.



1. INTRODUCTION

The global average concentration of atmospheric CO₂ has increased from preindustrial levels at around 280 ppm to the present-day level of 407 ppm within 260 years.^{1,2} The ever-increasing accumulation of CO₂ in the atmosphere has raised worldwide concern because of its strong connection to global warming, undesirable changes to climate, and environmental issues.^{3–5} Flue gas produced from the combustion of fossil fuels for power generation is the source of large-scale emissions of CO₂, accounting for approximately 33–40% of the global CO₂ emissions.^{6,7} As a result, a key need to realistically implement CO₂ capture, utilization, and storage (CCUS) technologies is to develop pre and postcombustion capture technologies such as absorption, adsorption, and membrane separations.^{8–10}

Currently, the most widely investigated process for CO₂ capture is absorption with conventional aqueous alkanolamines.^{11,12} However, a major problem associated with this process is the high energy consumption required for solvent regeneration. Membrane- and adsorption-based separations are regarded as promising and competitive alternative approaches because of their potentially lower energy consumption and ease of operation.^{13–22} In this regard, the development of advanced functional materials with superior separation

performance over traditional benchmarks is an integral step needed to enable CCUS.

Metal–organic frameworks (MOFs), an intriguing class of inorganic–organic porous crystalline materials, have been recognized as promising adsorbents and membrane fillers because of their high porosity, large surface area, and facile chemical functionality.^{23,24} Since the early demonstration of CO₂ adsorption in MOF-2,²⁵ a large number of MOF adsorbents with different organic linkers, pore sizes, and topologies have been investigated experimentally and computationally for CO₂ separations.^{26–28} Because of the presence of corrosive gases and water vapor in most industrial processes, chemically robust and water-resistant MOF adsorbents are highly desired.²⁹ Of particular interest is MIL-101(Cr), a mesoporous MOF composed of Cr₃O octahedral clusters linked by 1,4-benzenedicarboxylates, resulting in a zeotype architecture with an **mtn** topology.^{30–32} As shown in Figure 1,

Received: July 13, 2020

Revised: August 26, 2020

Accepted: August 28, 2020

Published: August 28, 2020

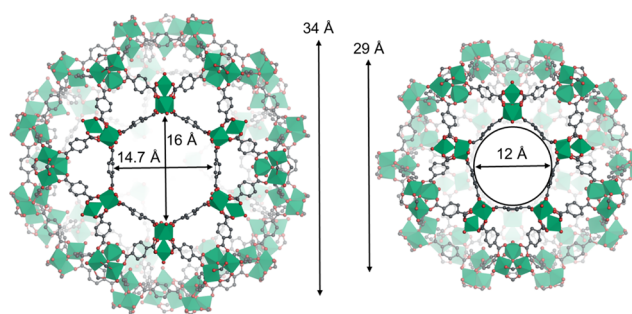


Figure 1. Schematic representation of the crystal structure of MIL-101(Cr). Trinuclear $\{\text{Cr}_3\text{O}\}$ building units and bridging terephthalic acid ligands form hexagonal (left) and pentagonal (right) rings, which are assembled into two types of mesoporous cages. Hydrogens are implicit.

two types of mesoporous quasi-spherical cages with an internal free diameter of ~ 29 and 34 \AA exist in MIL-101(Cr).^{30–32} This highly porous structure endows MIL-101(Cr) with enormous cell volumes around $702,000 \text{ \AA}^3$, numerous unsaturated chromium metal sites, and ultrahigh Brunauer–Emmett–Teller (BET) and Langmuir surface areas of approximately 4100 and $5900 \text{ m}^2/\text{g}$, respectively.^{30–33}

Several strategies can be applied to further optimize the physicochemical properties and CO_2 adsorption performance of MIL-101(Cr), including but not limited to tuning the pore size and shape, exposing the unsaturated metal sites, doping with alkali-metals, and functionalizing the organic ligands.^{34,35} Modeling studies show that the CO_2 uptake capacity and CO_2/N_2 selectivity of MIL-101(Cr) can be remarkably improved through amine functionalization.³⁶ The amine groups on the ligands of the framework can improve affinity to CO_2 molecules,^{37,38} and additionally, these groups can also provide chemical anchors for postsynthetic modification (PSM).^{39–42} However, direct synthesis of amine-functionalized MIL-101(Cr) through a single-step reaction is challenging because the 2-aminoterephthalic acid ligand is often incompatible with the reaction conditions necessary for MOF formation.^{43–46} To date, only a few studies have reported that amine-functionalized MIL-101(Cr) can be directly synthesized from the 2-aminoterephthalic acid ligand.^{44–46} Of note, these studies report MOF particles with significantly lower surface areas than those typically reported for the parent MIL-101(Cr) MOF.^{30,44–47} To the best of our knowledge, the highest reported BET surface area for amine-functionalized MIL-101(Cr) is $2258 \text{ m}^2/\text{g}$,⁴⁸ which is significantly less than its unfunctionalized counterpart.^{30,32} Therefore, while synthetic methods exist to form amine-functional MIL-101(Cr), none of these methods provides access to the expected high surface area of this MOF, which precludes experimental validation of separation performance limits in this material. Additionally, current synthesis methods frequently result in particle agglomerations, which would make it challenging to use these particles for mixed matrix membranes. Therefore, the development of simple and efficient synthetic routes for direct synthesis of high-quality amine-functionalized MIL-101(Cr) nanoparticles is highly desired by the adsorption and membrane community.

This work reports a facile and effective strategy for direct synthesis of amine-functionalized MIL-101(Cr) (i.e., MIL-101(Cr)-NH₂) nanoparticles with ultrahigh surface areas and minimized particle agglomerations. We thoroughly studied the

influence of reaction temperature and time, as well as pK_a value and concentration of the acid modulator on crystallinity, reaction yield, morphology, particle size, and surface area of MOF particles. Using these extensive characterization efforts, we provide a comprehensive study pinpointing the role of acid modulators and other reaction parameters on the direct formation of MIL-101(Cr)-NH₂. Owing to their high surface area and Lewis basic amine functionality, the MIL-101(Cr)-NH₂ nanoparticles exhibit exceptional CO_2 uptake capacity and high CO_2/N_2 selectivity, which surpasses other MIL-101(Cr) MOFs reported in the literature, suggesting their potential for CO_2 separations.

2. EXPERIMENTAL AND CHARACTERIZATION METHODS

2.1. MOF Synthesis and Purification. The MIL-101(Cr)-NH₂ nanoparticles were synthesized from $\text{Cr}(\text{NO}_3)_3 \cdot 9\text{H}_2\text{O}$ and 2-aminoterephthalic acid ($\text{H}_2\text{N}-\text{H}_2\text{BDC}$) in aqueous media using various inorganic and organic acids as the acidic modulators, including hydrochloric acid (HCl), nitric acid (HNO₃), acetic acid (CH₃COOH), trifluoroacetic acid (CF₃COOH), hydrofluoric acid (HF), and stearic acid. As tabulated in Table S1, the influence of reaction temperature and time, pK_a value of the acidic modulators, and acid/ $\text{H}_2\text{N}-\text{H}_2\text{BDC}$ molar ratio on MIL-101(Cr)-NH₂ formation were thoroughly investigated. For comparison, the MIL-101(Cr) benchmark was synthesized using terephthalic acid (H₂BDC) as the ligand following a method reported in our previous work.⁴⁶ The as-synthesized crude MOF particles were thoroughly washed using dimethylformamide (DMF) and ethanol and then activated at 150°C for 24 h under vacuum before characterization. A detailed description of MOF synthesis and purification can be found in the Supporting Information.

2.2. Characterization. The as-synthesized MIL-101(Cr)-NH₂ nanoparticles and MIL-101(Cr) benchmark were thoroughly characterized by powder X-ray diffraction (XRD), transmission electron microscopy (TEM), scanning electron microscopy (SEM), thermogravimetric analysis (TGA), X-ray photoelectron spectroscopy (XPS), and Fourier transform infrared (FTIR) spectroscopy. The N₂ adsorption–desorption isotherms for surface area measurements were conducted on a Micromeritics 3Flex apparatus at 77 K. The number-averaged particle size distribution was obtained from dynamic light scattering (DLS) analysis at 25°C . The details for sample preparation and analysis procedures are included in the Supporting Information.

2.3. Gas Adsorption Measurements. Adsorption isotherms of the MOF nanoparticles for CO_2 , CH₄, and N₂ were measured on a Micromeritics 3Flex apparatus using ultrahigh purity gases from Airgas. For each measurement, 100–150 mg of the sample was used and the sample was activated at 150°C for at least 12 h. Detailed testing conditions and procedures are described in the Supporting Information. The relationship between the uptake amount and gas bulk pressure was obtained using a Langmuir–Freundlich (L–F) fit for the adsorption isotherms.^{49–52}

$$\frac{N}{N_m} = \frac{B \times P^{(1/t)}}{1 + B \times P^{(1/t)}} \quad (1)$$

where N and N_m represent the adsorption amount and the theoretical maximum uptake at a certain equilibrium pressure

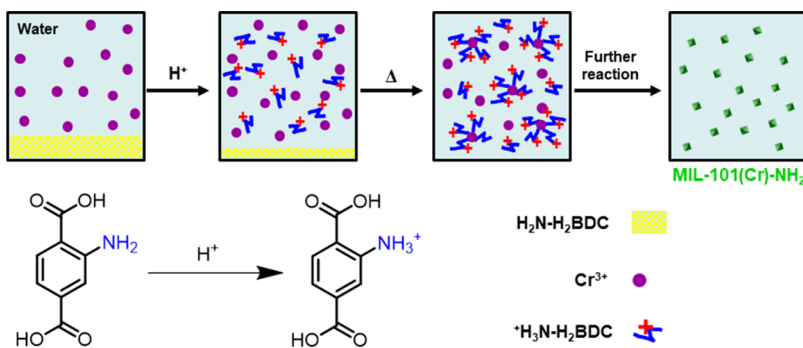


Figure 2. Procedure to synthesize MIL-101(Cr)-NH₂ nanoparticles in water using an acid modulator.

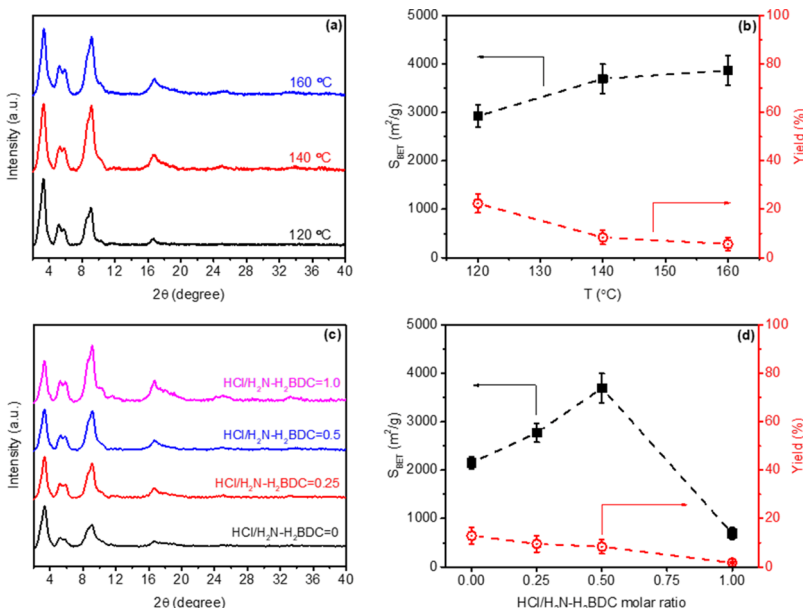


Figure 3. Powder XRD patterns (a,c) and BET surface area and reaction yield (b,d) of the MIL-101(Cr)-NH₂ nanoparticles. In figures (a,b), the particles were synthesized at different temperatures using an HCl modulator with an HCl/H₂N-H₂BDC molar ratio of 0.5. In figures (c,d), the particles were synthesized at 140 °C using an HCl modulator with different HCl/H₂N-H₂BDC molar ratios. The reaction time for all syntheses was 24 h.

(P), respectively. Both B and t are the equation constants. The obtained adjusted R²-values for all of these fits were larger than 0.999. The above equation can be rewritten to obtain the accurate pressure, P, corresponding to the same adsorption amount.

$$P = \left(\frac{N/N_m}{B - B \times N/N_M} \right)^t \quad (2)$$

The single gas ideal selectivity (α) of gas A over gas B at a certain pressure was calculated as

$$\alpha_{A/B} = \frac{N_A}{N_B} \quad (3)$$

The zero-coverage isosteric heat (Q_{st}) of CO₂ adsorption was calculated from the Clausius–Clapeyron equation^{50,52}

$$\frac{d\ln P}{d(1/T)} = -\frac{Q_{st}}{R} \quad (4)$$

The adsorption selectivity factor (S_{ads}) for binary gas mixtures of CO₂ and N₂ was obtained using ideal adsorbed solution theory (IAST)⁵²

$$S_{ads} = \frac{q_{CO_2}/q_{N_2}}{p_{CO_2}/p_{N_2}} \quad (5)$$

where q_i is the uptake and p_i is the partial pressure of component i. An idealized post-combustion flue gas mixture composed of 0.15 bar CO₂ and 0.85 bar N₂ was used in this study to calculate the IAST selectivities at 323 K.⁵² The procedures for gas adsorption measurements and data analysis are similar to our previous work,⁴⁶ and detailed procedures for the current study can be found in the Supporting Information.

3. RESULTS AND DISCUSSION

3.1. Synthesis of MIL-101(Cr)-NH₂ Nanoparticles. As illustrated in Figure 2, hydrothermal reactions of Cr(NO₃)₃·9H₂O and H₂N-H₂BDC in water were used to directly synthesize MIL-101(Cr)-NH₂. Unlike terephthalic acid, which is used for the synthesis of the parent MIL-101(Cr), H₂N-H₂BDC is an aromatic amino diacid that is well known to form zwitterions depending on solution pH.⁵³ The presence of amine groups changes the Brønsted acid–base properties and thermal stability of the carboxylic acid,^{43,45} and therefore, using the zwitterionic H₂N-H₂BDC as a ligand significantly

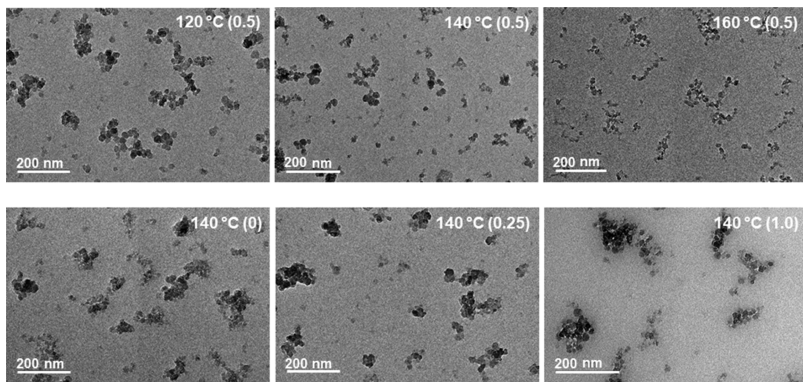


Figure 4. TEM images of MIL-101(Cr)-NH₂ synthesized at different temperatures using an HCl modulator with an HCl/H₂N-H₂BDC molar ratio of 0.5 (top) and MIL-101(Cr)-NH₂ synthesized at 140 °C using an HCl modulator with different HCl/H₂N-H₂BDC molar ratios that are indicated in the figure parentheses (bottom). The reaction time for all syntheses was 24 h.

complicates MOF synthesis. To minimize the influence of the amine groups during MOF synthesis, acids were selected as modulators to protonate the amines. For hydrothermal reactions, protonation of the H₂N-H₂BDC ligand was expected to improve ligand solubility and reduce particle aggregation via charge repulsion during synthesis.⁵⁴ On the other hand, the acid modulator was expected to suppress the deprotonation rate of the carboxylic acids, which may help prevent the formation of amorphous impurities and reduce particle size.^{55,56}

Because the reaction temperature has a profound impact on the pK_a of the acid modulator, the dissociation of carboxylic acids, and the solubility of the ligand, it likewise has an impact on the nucleation and growth of MOF crystals. Therefore, the influence of reaction temperature on the formation of MIL-101(Cr)-NH₂ was investigated by raising the temperature systematically from 120 to 180 °C at a constant reaction time of 24 h (Table S1). HCl was used as the probe modulator, and the HCl/H₂N-H₂BDC molar ratio was kept at 0.5. XRD patterns in Figure 3a show that the as-prepared MIL-101(Cr)-NH₂ particles have similar Bragg diffraction patterns for all reaction temperatures considered. Moreover, these patterns are nearly identical to those of the parent MIL-101(Cr) MOF,³² confirming the presence of an intact MIL-101 crystal structure. At the same time, the reaction temperature shows a direct influence on the reaction yield and particle BET surface area. As depicted in Figure 3b, the synthesis conducted at a relatively low temperature of 120 °C had the highest reaction yield. With the increasing reaction temperature, the yield rapidly decreases and became exceedingly low at 160 °C, likely because of the suppressed deprotonation of the carboxylic acid ligands by HCl at higher temperatures.

In contrast with the reaction yield, the BET surface area increases significantly with increasing temperature, where high surface areas of $3700 \pm 200 \text{ m}^2/\text{g}$ and $3900 \pm 100 \text{ m}^2/\text{g}$ were achieved at 140 and 160 °C, respectively (Figures 3b and S1). In general, higher BET surface areas correlated with smaller and better-dispersed particles. As presented in Figures 4 and S2–S4, all of the MIL-101(Cr)-NH₂ nanoparticles possess extremely small particle sizes that are in the sub-20 nm range, which approximately matches the particle size calculated by the Scherrer equation from XRD patterns (i.e., 15–18 nm).⁵⁷ A visible decrease in the particle size and aggregation was observed with increasing reaction temperature, and the 160 °C synthesis resulted in the smallest particle sizes of approximately

15 nm. This finding likely results from the charge-induced repulsion by the protonated amine groups on the ligands by HCl, which is consistent with the reaction scheme presented in Figure 2. Owing to their small particle size, the MIL-101(Cr)-NH₂ nanoparticles show excellent dispersibility in ethanol, where a very stable suspension is formed (Figure S5a).

Another factor that could significantly influence the formation of MIL-101(Cr)-NH₂ is acid concentration, which was further investigated by performing a number of reactions at 140 °C for 24 h with different HCl/H₂N-H₂BDC molar ratios (Table S1). The XRD patterns in Figure 3c imply that MIL-101(Cr)-NH₂ is formed when the HCl/H₂N-H₂BDC molar ratios are less than or equal to 1.0. However, the molar ratio significantly affects the reaction yield and particle surface area. As shown in Figures 3d and S1, the reaction yield decreases monotonically with the increase of HCl/H₂N-H₂BDC molar ratios, while the BET surface area first increases, reaching the highest value of $3700 \pm 200 \text{ m}^2/\text{g}$ at a molar ratio of 0.5 and then rapidly decreases to $700 \pm 100 \text{ m}^2/\text{g}$ at a molar ratio of 1.0. We also found that increasing the reaction time from 24 to 72 h failed to improve the particle surface area (Figure S6), while degradation of the MOF building blocks occurred as indicated by the brown color of the formed particle suspensions (Figure S5b).

TEM images further show that the size and agglomeration of the formed MIL-101(Cr)-NH₂ nanoparticles are notably influenced by the HCl/H₂N-H₂BDC molar ratio. As presented in Figures 4 and S7–S10, a slight reduction in particle size and some particle agglomeration result from the addition of the HCl modulator. The most well-defined MIL-101(Cr)-NH₂ nanoparticles were obtained at a molar ratio of 0.5, which corresponds with the highest surface area samples for this series of tests. However, further increasing the molar ratio to 1.0 results in a light brown color of the particle suspension (Figure S5b), suggesting the formation of some amorphous impurities. At an even a higher HCl/H₂N-H₂BDC molar ratio of 2.0, clear evidence of amorphous solids was found from the XRD spectra and TEM images (Figures S11–S13), independent of the reaction temperature and time. These findings indicate that the addition of excess acid prevents sufficient deprotonation of the carboxylic acid, thereby preventing nucleation and growth conditions needed to synthesize high fidelity crystals. Moreover, the low BET surface areas of 400 ± 50 and $500 \pm 50 \text{ m}^2/\text{g}$ also suggest structures that are largely amorphous (Figure S11). The dark black color of the particles

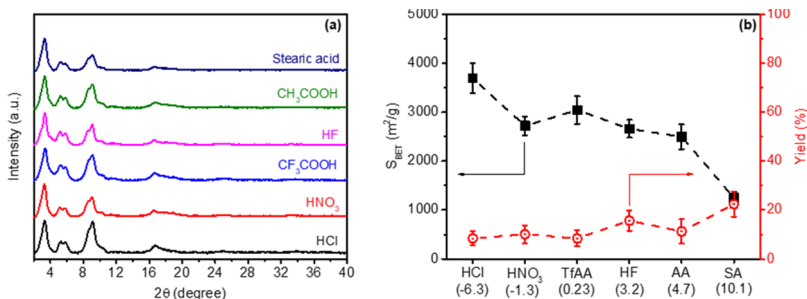


Figure 5. Powder XRD patterns (a) and BET surface area and reaction yield (b) of MIL-101(Cr)-NH₂ synthesized using different acids as modulators. All reactions were performed at 140 °C for 24 h and the molar ratio of each acid to H₂N-H₂BDC is 0.5. The pK_a values of the acids are shown in figure parentheses. TfAA, AA, and SA represent trifluoroacetic acid, acetic acid, and stearic acid, respectively.

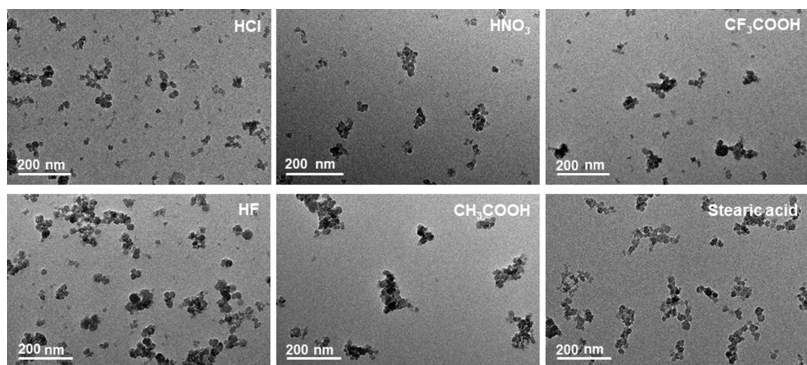


Figure 6. TEM images of MIL-101(Cr)-NH₂ synthesized at 140 °C for 24 h using different acids as the modulators. The molar ratio of each acid to H₂N-H₂BDC is 0.5.

formed at 180 °C indicates degradation of the H₂N-H₂BDC ligand at this temperature because of its relatively low thermal stability (Figure S11b).⁴³

3.2. Effects of Acidic Modulator on the Formation of MIL-101(Cr)-NH₂. Inorganic and organic acid modifiers, such as HF, HCl, HNO₃, H₂SO₄, HCOOH, CH₃COOH, CF₃COOH, stearic acid, and benzoic acid, have been widely used for the synthesis of the unfunctionalized MIL-101(Cr) analogue and other MOFs.^{55–59} The acidic modulators are assumed to be capable of modulating MOF crystal growth by tuning the reaction kinetics. A similar phenomenon was observed in this study for the direct synthesis of MIL-101(Cr)-NH₂ from H₂N-H₂BDC. The experimental data presented above have demonstrated that HCl can effectively modulate the formation of MIL-101(Cr)-NH₂ nanoparticles, where the HCl/H₂N-H₂BDC molar ratio plays critical roles in the quality of the formed particles. As illustrated in Figure 2, the addition of an HCl modulator is expected to improve the solubility of the H₂N-H₂BDC ligand in aqueous media through amine protonation. Figure S14 shows that the H₂N-H₂BDC ligand is almost insoluble in water, while the Cr(NO₃)₃·9H₂O metal precursor can be fully dissolved, resulting in a heterogeneous reaction solution for MIL-101(Cr)-NH₂ synthesis. The addition of HCl improves the ligand solubility, where H₂N-H₂BDC can almost be fully dissolved at an HCl/H₂N-H₂BDC molar ratio of 2.0. The enhanced solubility of H₂N-H₂BDC provides more free ligands in the solution to interact with the chromic metal ions for MOF formation. On the other hand, the addition of HCl suppresses the deprotonation of carboxylic acid in H₂N-H₂BDC, which is unfavorable for nucleation and growth of MIL-101(Cr)-NH₂ crystals. As shown in Figure S14, no precipitate is formed when the Cr(NO₃)₃·9H₂O is mixed

with the dissolved H₂N-H₂BDC ligands at room temperature. Thus, ligand solubility can be attributed to the protonation of the amine, and increases in reaction temperature are required to shift the reaction equilibrium to favor carboxylate formation and MOF nucleation and growth. In other words, the dissociation of the carboxylic acids on 2-aminoterephthalic acid is too weak to provide sufficient reactivity for crystal formation at room temperature, and for high HCl concentrations (e.g., 2/1 molar ratios of HCl/H₂N-H₂BDC), deprotonation is unfavorable at all accessible reaction temperatures and times (Figures S11–S13).

In addition to HCl, other acidic modulators with a wide range of pK_a values were also investigated for the formation of MIL-101(Cr)-NH₂. As displayed in Figure 5a, crystalline MIL-101(Cr)-NH₂ nanoparticles are formed for all syntheses performed at 140 °C for 24 h using different acidic modulators with an acid/H₂N-H₂BDC molar ratio of 0.5, suggesting that the pK_a value of the acid modulator has a minor influence on the particle crystalline structure. However, the identity of the acid significantly influences the reaction yield and particle surface area. As depicted in Figures 5b and S15, HCl (which has the lowest pK_a value among the acidic modulators) shows the highest surface area and lowest yield. The reaction yield increases, while the surface area decreases with increasing pK_a value of the modulator. In particular, stearic acid (a saturated fatty acid with the highest pK_a value considered) results in particles with the lowest surface area but the highest yield. These data are consistent with our hypothesis that the pK_a value of the acidic modulator has a direct influence on the trade-off relationship between the protonation of amine groups and deprotonation of the carboxylic acids. In addition, TEM images in Figures 6 and S16–20 show that the MIL-101(Cr)-

NH_2 nanoparticles modulated by HCl have the smallest average particle size with the lowest agglomeration, implying that strong acids are favorable modulators for the formation of high-quality MIL-101(Cr)- NH_2 nanoparticles.

In terms of adsorption applications, functionalized MOFs provide several potential advantages, such as having added chemical functionality that can selectively manipulate adsorbent–adsorbate interactions and, after they are formed, having PSM capabilities to enable their compatibility and interaction with binders.^{28,42,60} However, adding these types of functionalities significantly complicates MOF synthesis, and MIL-101(Cr)- NH_2 provides a representative example of one of these systems. Thus, our detailed systematic study of reaction conditions provides not only an optimized recipe for this MOF material but also general guidelines that can be applied to the synthesis of other MOF materials with similar structural features.

3.3. Characterization of MIL-101(Cr)- NH_2 Nanoparticles. For the remainder of this report, we will focus on the MIL-101(Cr)- NH_2 synthesized at 140 °C for 24 h with an HCl/ $\text{H}_2\text{N}-\text{H}_2\text{BDC}$ molar ratio of 0.5, which had the highest surface area with an acceptable yield. The parent MIL-101(Cr), prepared as the benchmark for comparison, has been reported in our previous study.⁴⁶ Figure 7 shows the TEM and

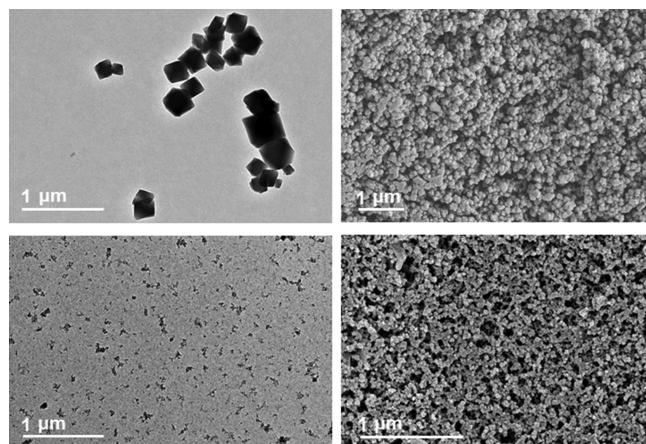


Figure 7. TEM and SEM images of the parent MIL-101(Cr) benchmark (top) and MIL-101(Cr)- NH_2 (bottom).

SEM images of MIL-101(Cr)- NH_2 and the MIL-101(Cr) benchmark. Distinct differences in particle shape, size, and size uniformity are observed. Compared to the parent MIL-101(Cr) benchmark, the synthesized MIL-101(Cr)- NH_2 particles show sphere-like morphology and ultra-small particle sizes of less than 20 nm with good size uniformity. Figure S21 presents the particle size distributions of two samples as measured by DLS. The MIL-101(Cr) particles were approximately 105–300 nm in size, which matches the dimensions characterized by TEM and SEM; while the MIL-101(Cr)- NH_2 nanoparticles were approximately 50–100 nm. Compared to the observations from TEM, the relatively larger hydrodynamic diameters calculated by DLS measurements are mainly due to agglomeration of the tiny nanoparticles during the measurements.

XRD patterns in Figure 8a show that the diffraction peaks for MIL-101(Cr)- NH_2 closely match those of the MIL-101(Cr) benchmark and the simulated crystal structure.³² Some key differences are the rather broad diffraction peaks and

the relatively low peak intensity of MIL-101(Cr)- NH_2 , which is indicative of small particle size. The estimated crystallite size based on the Scherrer equation is approximately 15–20 nm, which closely matches particle sizes observed from the SEM and TEM images. FTIR analysis shows the presence of amine groups in the MIL-101(Cr)- NH_2 framework. As shown in Figure 8b, the emerging double peaks at 3490 and 3380 cm⁻¹ are attributed to the asymmetric and symmetric vibrations of the – NH_2 groups, respectively, while the peaks at 1593 and 1340 cm⁻¹ correspond to –N–H bending and –C–N stretching on the aromatic ring, respectively.⁴³ XPS elemental analysis in Figure 8c demonstrates the existence of N 1s and Cr 2p peaks at 399.2 and 577.1 eV, respectively, which are ascribed to aromatic amines and CrO in the MIL-101(Cr)- NH_2 framework. Additionally, an N/Cr atomic ratio of approximately 1.1 is observed for MIL-101(Cr)- NH_2 , which is close to the theoretical value of 1.0.³² The slight deviation in the N/Cr atomic ratio is possible because of sample contamination during the XPS tests and trace amounts of residual DMF solvent in the pores. TGA analysis in Figure 8d shows that the MIL-101(Cr)- NH_2 particles have excellent thermal stability similar to that of the parent MIL-101(Cr) MOF. The weight-loss step (~73%) that occurred between 250 and 350 °C corresponds to the loss of coordinated solvents and the decomposition of the framework.⁴⁴

Figure 9a shows that MIL-101(Cr)- NH_2 has a similar N_2 adsorption–desorption isotherm to that of the MIL-101(Cr) benchmark, which is expected based on their isostructural topology.^{43,61} MIL-101(Cr)- NH_2 has a BET and Langmuir surface area of 3700 ± 200 and $5400 \pm 200 \text{ m}^2/\text{g}$, respectively, surpassing those of the parent MIL-101(Cr) benchmark synthesized in this study (i.e., 2700 ± 100 and $4000 \pm 200 \text{ m}^2/\text{g}$). The pore size distribution curves in Figure 9b show three prominent pores for the parent MIL-101(Cr) framework centered at approximately 11, 23, and 31 Å. These results match pore size distributions reported for other MIL-101(Cr) MOFs and closely match the corresponding pore sizes estimated from the crystal structure.^{33,55,56} Because of the presence of amine groups projecting into the pores, a slight decrease in pore size distribution was observed for the MIL-101(Cr)- NH_2 framework relative to that of MIL-101(Cr).⁴⁵ The higher baseline for MIL-101(Cr)- NH_2 at larger pore width suggests the presence of large textural pores created by the aggregation of nanoparticles during activation and drying, which is in good agreement with the hysteresis in corresponding isotherms. To the best of our knowledge, the newly developed MIL-101(Cr)- NH_2 nanoparticles have the highest BET surface area (as summarized in Figure S22) compared to other reported MIL-101(Cr)- NH_2 MOFs that are directly synthesized from the 2-aminoterephthalic acid,^{44,45} making these particles of interest for adsorption-based applications. Additionally, these nanoparticles are also the smallest among the reported MIL-101(Cr)- NH_2 , making them of particular interest for mixed-matrix membranes that require small nanoparticles to make thin films.

3.4. MIL-101(Cr)- NH_2 for CO₂ Separations. CO₂ capture from natural gas and coal-fired power plants has attracted great interest because of environmental concerns over climate change.^{1,27} The CO₂ separation performance of the newly synthesized MIL-101(Cr)- NH_2 was therefore evaluated by comparing their adsorption isotherms for CO₂, CH₄, and N₂ at different temperatures and pressures. The same measurements

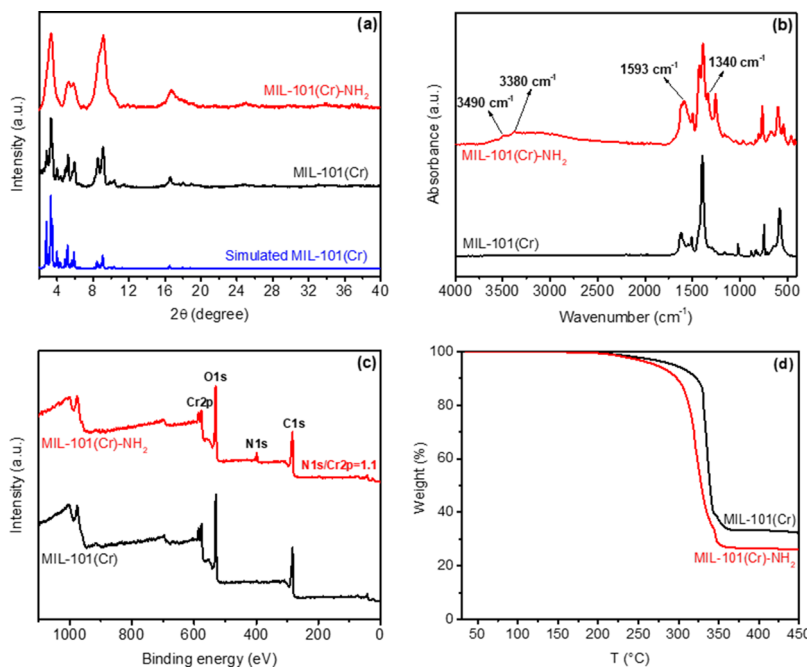


Figure 8. Powder XRD (a), FTIR (b), XPS (c), and TGA (d) patterns of the MIL-101(Cr) benchmark and MIL-101(Cr)-NH₂.

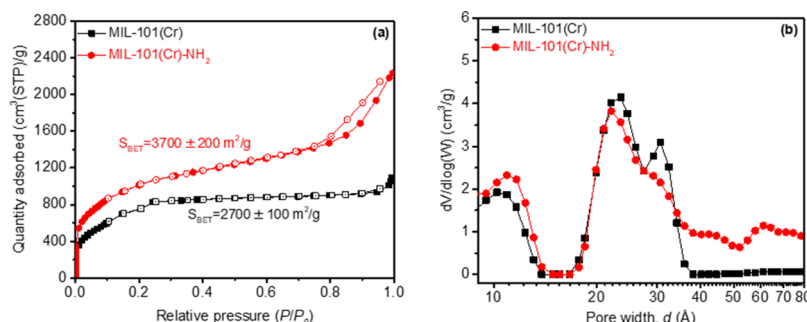


Figure 9. N₂ adsorption–desorption isotherms at 77 K (a) and pore size distribution curves (b) of the MIL-101(Cr) benchmark and MIL-101(Cr)-NH₂.

were conducted on the parent MIL-101(Cr) benchmark for comparison.

Figure 10 shows the CO₂, CH₄, and N₂ adsorption isotherms at 308 K and the calculated ideal selectivity for the MIL-101(Cr) benchmark and MIL-101(Cr)-NH₂. Both compounds show much higher uptakes for CO₂ than CH₄ and N₂ at all testing pressures, which follows other reported trends for this family of MOFs.^{33–36} At each pressure, CO₂ adsorption capacity in MIL-101(Cr)-NH₂ is much higher than that in the MIL-101(Cr) benchmark. For example, high CO₂ uptake of 3.1 mmol/g was achieved for MIL-101(Cr)-NH₂ at 750 mmHg, which is approximately 1.8 times higher than that of its unfunctionalized analogue. Figure 10 also shows that the N₂ uptake is similar for both samples and much lower than that of CO₂ at all testing pressures, suggesting that the amine functional groups on the framework can selectively adsorb CO₂ over N₂. As a consequence, a high ideal CO₂/N₂ selectivity of 12.4 was achieved for MIL-101(Cr)-NH₂ at 750 mmHg (Figure 10 and Table S2). At a lower testing pressure of 75 mmHg, the ideal selectivity can be improved to 32.5, representing a 65% improvement in CO₂/N₂ selectivity compared to the parent MIL-101(Cr) benchmark (Figure 10 and Table S2). In contrast, both samples exhibit similar CO₂/

CH₄ selectivity, although MIL-101(Cr)-NH₂ has higher CO₂ uptake than the parent framework. This finding corresponds with the greater polarizability of CH₄ than N₂.^{36,43}

To further elaborate the influence of amine functional groups on gas adsorption, CO₂, CH₄, and N₂ adsorption isotherms at 308 K for MIL-101(Cr)-NH₂ and the MIL-101(Cr) benchmark were replotted based on per unit internal surface area. This analysis effectively removes sample-to-sample differences in adsorption that result from differences in surface areas and, instead, permits a direct comparison of how the amine functional groups influence adsorption in these samples. As displayed in Figure 11a, the equilibrium CO₂ uptake per unit surface area is similar for both samples at low pressures, which indicates that the strong binding of CO₂ with the unsaturated chromium metal sites exists in both MOFs and is the primary binding mechanism. At higher pressures, however, MIL-101(Cr)-NH₂ shows significantly higher CO₂ uptake than that of the MIL-101(Cr) benchmark. In contrast, similar CH₄ and N₂ uptake is observed at all pressures for both MOFs, as shown in Figure S23. From this perspective, it is clear that the enhanced total CO₂ adsorption capability in MIL-101(Cr)-NH₂ is partially due to the amine functional groups and not only related to the higher internal surface area

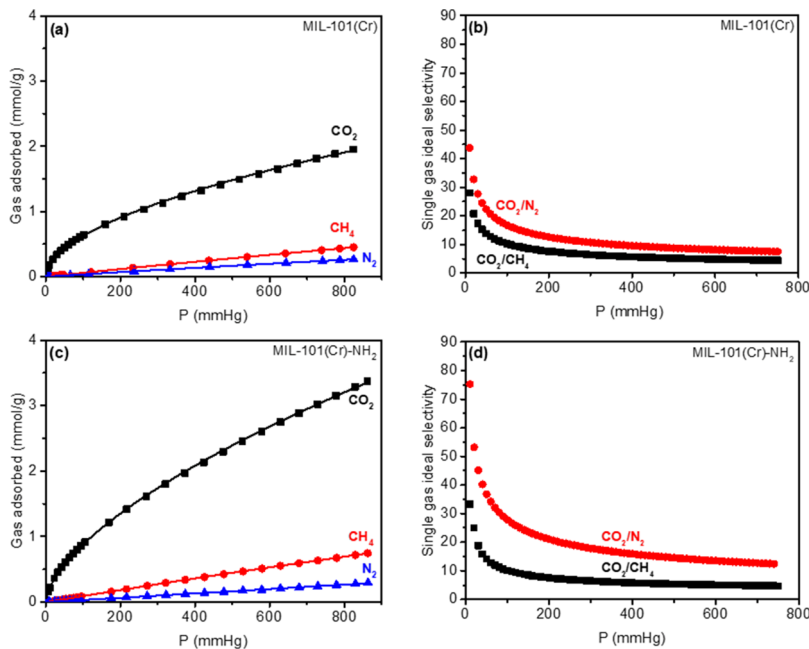


Figure 10. CO₂, CH₄, and N₂ adsorption isotherms at 308 K and the calculated single gas ideal selectivity for the MIL-101(Cr) benchmark (a,b), and MIL-101(Cr)-NH₂ (c,d). The solid lines in figures (b,c) are the fitted curves using the L-F model.

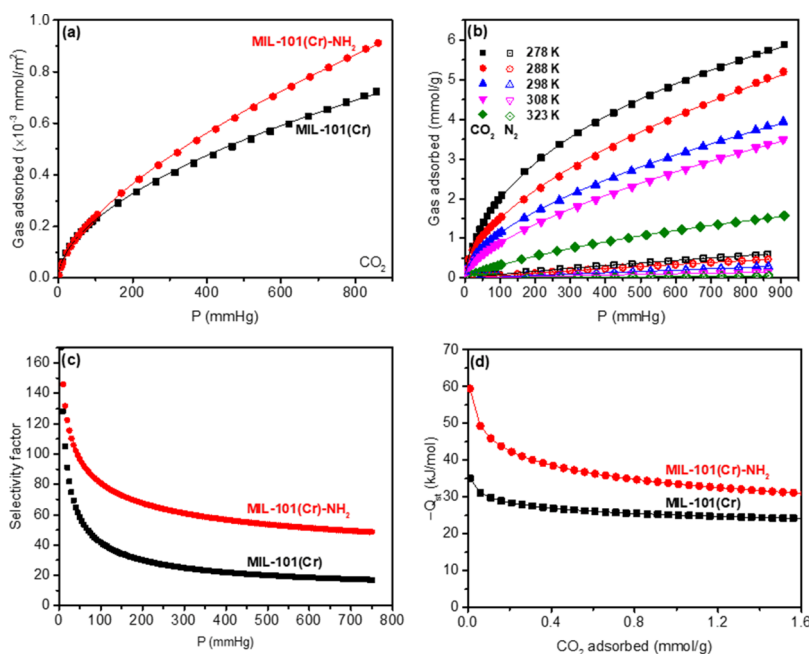


Figure 11. CO₂ adsorption isotherms on a per unit internal surface area basis at 308 K for MIL-101(Cr)-NH₂ and the MIL-101(Cr) benchmark (a), CO₂ and N₂ adsorption isotherms for MIL-101(Cr)-NH₂ measured from 278 to 323 K (b), the calculated IAST selectivities for a CO₂/N₂ binary mixture with a 15:85 mixture composition at 323 K (c), and isosteric heats for CO₂ adsorption for MIL-101(Cr)-NH₂ and the MIL-101(Cr) benchmark (d). Solid lines in figures (a,b) are the fitted curves using the L-F model.

of the sample. From an electrostatic perspective, the partial negative charge on the amino nitrogen (-0.965 e) can interact favorably with the partial positive charge of carbon (0.6645 e) in CO₂. Additionally, the hydrogens in $-\text{NH}_2$ can form hydrogen bonds with oxygens in CO₂.³⁶ Therefore, CO₂ can be further accommodated near the $-\text{NH}_2$ groups in MIL-101(Cr)-NH₂, which significantly enhances CO₂ uptake. Moreover, in contrast with the unsaturated metal sites, which are the primary binding sites in MIL-101(Cr) MOFs, amine functional groups have been shown to enable CO₂ capture in

the presence of water.⁶² Therefore, these features can enhance the feasibility of MIL-101(Cr)-NH₂ for practical capture processes, especially for working capacities across a range of gas-phase compositions where the open metal site is saturated with water.

Figures 11b and S24 show the CO₂ and N₂ adsorption isotherms measured at temperatures from 278 to 323 K for MIL-101(Cr)-NH₂ and the MIL-101(Cr) benchmark. At a lower temperature of 278 K, the CO₂ uptake for MIL-101(Cr)-NH₂ reaches 5.4 mmol/g at 750 mmHg, which is

Table 1. Comparison of CO₂ Adsorption for Various Relevant Materials

adsorbent	CO ₂ uptake (mmol/g)	pressure (bar)	temperature (K)	-Q _{st} (kJ/mol)	references
MIL-101(Cr)-NH ₂	5.4	1.0	278	59.5	this work
MIL-101(Cr)-NH ₂	3.3	1.0	273	50.1	44
MIL-101(Cr)-NH ₂	3.0	1.0	273		45
MIL-101(Cr)-NH ₂	2.0	0.15	273	43	73
MIL-101(Cr)	3.8	1.1	288	38.8	33
MIL-101(Cr)	1.2	1.0	298	21.0	74
MIL-101(Cr)	1.6	1.0	298		75
MIL-100(Cr)	5.0	5.0	303	63	76
Cu-BTTri	3.2	1.0	298	21	77
HKUST-1	4.7	0.9	295	35	78
Mg-MOF-74	8.0	1.0	296	47	69
IRMOF-3	1.2	1.1	298		79
MIL-101-53-NH ₂	2.3	5.0	303	38.4	80
MIL-101-125-NH ₂	4.0	1.0	273	31	81
zeolite LiX	4.64	1.0	293	71	82
activated carbon	2.76	1.0	293	35	82

approximately 1.9 times higher than that of the MIL-101(Cr) benchmark. This uptake for CO₂ is higher than that of other reported MIL-101(Cr) MOFs under similar testing conditions (Table 1). For flue gas, CO₂ is typically released at a partial pressure of approximately 0.15 bar (or 112.5 mmHg).⁶³ As a result, the adsorption capacity for CO₂ in the low-pressure region is critically important when developing process models for postcombustion CO₂ capture. At this pressure and 278 K, MIL-101(Cr)-NH₂ adsorbs 2.13 mmol/g CO₂ (Figure 11b), while the corresponding uptake capacity for the MIL-101(Cr) benchmark is only 1.09 mmol/g (Figure S24). The IAST estimations of adsorption selectivities for CO₂ over N₂ were also calculated for an idealized flue gas mixture composed of 0.15 bar CO₂ and 0.85 bar N₂ based on the fits to the isotherms at 323 K. As shown in Figure 11c and Table S3, MIL-101(Cr)-NH₂ demonstrates tremendous selectivities at various pressures, with an IAST selectivity factor of 122.0 at 20 mmHg and 48.6 at 750 mmHg, respectively, which are much higher than those of the MIL-101(Cr) benchmark and outperform other reported MOFs under similar conditions such as DMOF-Cl₂ (selectivity = 28),⁶⁴ Zn/Ni-ZIF-8-1000 (selectivity = 30),⁶⁵ ZnF(TZ) (selectivity = 25),⁶⁶ LIFM-33 (selectivity = 30),⁶⁷ and modified UiO-66 (selectivity = 19.1–33.3).⁶⁸

The isosteric heat (Q_{st}) of CO₂ adsorption for MIL-101(Cr)-NH₂ was calculated using the Clausius–Clapeyron equation and compared with that of the MIL-101(Cr) benchmark to quantify how the enhanced CO₂ capture ability could potentially translate to a thermal swing process. As shown in Figure 11d, Q_{st} is around -59.5 kJ/mol for MIL-101(Cr)-NH₂ at the onset of adsorption, which is among the highest Q_{st} values for amine-functionalized MOFs reported in the literature (Table 1).^{69–72} In contrast, the unfunctionalized analogue shows a much lower Q_{st} of around -35.1 kJ/mol, implying its more mild affinity to CO₂. Note that this Q_{st} value for the parent framework is also in good agreement with literature values.³³ With the increase of pressure, CO₂ adsorption becomes less favorable and the adsorbate–adsorbent interaction becomes weaker. Thus, the effects of the amine groups become less pronounced as these adsorption sites are saturated. As a result, Q_{st} becomes less exothermic and more similar for the amine-functional and parent frameworks at higher pressures. Both the isosteric heats and the adsorption

performance demonstrate that the superior CO₂ uptake in MIL-101(Cr)-NH₂ is mainly due to the strong interaction between CO₂ and the amine functionality. These results indicate that careful control of acid-modulated synthesis can enable the formation of amine-functionalized MOFs with excellent CO₂ separation capabilities.

4. CONCLUSIONS

This work describes a facile and effective strategy for direct synthesis of high surface area amine-functionalized MIL-101(Cr) nanoparticles for applications in CO₂ separations. We demonstrated that an acidic modulator could significantly reduce particle size and increase particle surface area through protonation of the amine groups on H₂N-H₂BDC ligands. Protonation improved ligand solubility in water and promoted nucleation while suppressing particle agglomeration via charge repulsion. The as-prepared amine-functionalized MIL-101(Cr) nanoparticles have ultrahigh BET and Langmuir surface areas of 3700 ± 200 and $5400 \pm 200 \text{ m}^2/\text{g}$, respectively. To the best of our knowledge, these values represent the highest surface areas that have been reported for amine-functionalized MIL-101(Cr). Owing to their amine functionality and high surface area, the synthesized MIL-101(Cr) nanoparticles have high CO₂ uptakes and excellent CO₂/N₂ selectivity. The high Q_{st} value of -59.5 kJ/mol for CO₂ adsorption indicates the strong interaction between CO₂ molecules and the amine-functionalized framework. The successful preparation of high surface area amine-functionalized MIL-101(Cr) MOFs could enable new opportunities for advanced functional MOF adsorbents and MOF-based membranes for CO₂ separations.

■ ASSOCIATED CONTENT

SI Supporting Information

The Supporting Information is available free of charge at <https://pubs.acs.org/doi/10.1021/acs.iecr.0c03456>.

Chemicals and detailed procedures for the synthesis and purification of MIL-101(Cr)-NH₂ and MIL-101(Cr) nanoparticles; characterization methods and procedures; gas adsorption tests; additional TEM images; XRD patterns; DLS particle size distribution curves; N₂ adsorption–desorption isotherms at 77 K; CO₂, CH₄, and N₂ adsorption isotherms; and the calculated selectivity (PDF)

AUTHOR INFORMATION

Corresponding Author

Zachary P. Smith — Department of Chemical Engineering, Massachusetts Institute of Technology, Cambridge, Massachusetts 02139, United States; [0000-0002-9630-5890](https://orcid.org/0000-0002-9630-5890); Phone: +1 6177154503; Email: zpsmith@mit.edu; Fax: +1 6172588224

Authors

Gang Han — Department of Chemical Engineering, Massachusetts Institute of Technology, Cambridge, Massachusetts 02139, United States; [0000-0001-8943-569X](https://orcid.org/0000-0001-8943-569X)

Katherine Mizrahi Rodriguez — Department of Materials Science and Engineering, Massachusetts Institute of Technology, Cambridge, Massachusetts 02139, United States; [0000-0002-5366-3743](https://orcid.org/0000-0002-5366-3743)

Qihui Qian — Department of Chemical Engineering, Massachusetts Institute of Technology, Cambridge, Massachusetts 02139, United States

Complete contact information is available at:

<https://pubs.acs.org/10.1021/acs.iecr.0c03456>

Notes

The authors declare no competing financial interest.

ACKNOWLEDGMENTS

The authors gratefully acknowledge the financial support from the Abdul Latif Jameel Water and Food Systems Lab (J-WAFS) at MIT.

REFERENCES

- (1) Wang, J.; Huang, L.; Yang, R.; Zhang, Z.; Wu, J.; Gao, Y.; Wang, Q.; O'Hare, D.; Zhong, Z. Recent Advances in Solid Sorbents for CO₂ Capture and New Development Trends. *Energy Environ. Sci.* **2014**, *7*, 3478–3518.
- (2) *State of the Climate in 2017*; Blunden, J., Arndt, D. S., Hartfield, G., Eds.; Bulletin of the American Meteorological Society, 2018; Vol. 99 (8), Si–S332.
- (3) Gattuso, J.-P.; Magnan, A.; Billé, R.; Cheung, W. W. L.; Howes, E. L.; Joos, F.; Allemand, D.; Bopp, L.; Cooley, S. R.; Eakin, C. M.; Hoegh-Guldberg, O.; Kelly, R. P.; Pörtner, H.-O.; Rogers, A. D.; Baxter, J. M.; Laffoley, D.; Osborn, D.; Rankovic, A.; Rochette, J.; Sumaila, U. R.; Treyer, S.; Turley, C. Contrasting Futures for Ocean and Society from Different Anthropogenic CO₂ Emissions Scenarios. *Science* **2015**, *349*, aac4722.
- (4) Schleussner, C.-F.; Rogelj, J.; Schaeffer, M.; Lissner, T.; Licker, R.; Fischer, E. M.; Knutti, R.; Levermann, A.; Frieler, K.; Hare, W. Science and Policy Characteristics of the Paris Agreement Temperature Goal. *Nat. Clim. Change* **2016**, *6*, 827–835.
- (5) Fuglestvedt, J.; Berntsen, T.; Eyring, V.; Isaksen, I.; Lee, D. S.; Sausen, R. Shipping Emissions: From Cooling to Warming of Climate-and Reducing Impacts on Health. *Environ. Sci. Technol.* **2009**, *43*, 9057–9062.
- (6) Yang, H.; Xu, Z.; Fan, M.; Gupta, R.; Slimane, R. B.; Bland, A. E.; Wright, I. Progress in Carbon Dioxide Separation and Capture: A review. *J. Environ. Sci.* **2008**, *20*, 14–27.
- (7) Nemitallah, M. A.; Abdelhafez, A. A.; Ali, A.; Mansir, I.; Habib, M. A. Frontiers in Combustion Techniques and Burner Designs for Emissions Control and CO₂ Capture: A Review. *Int. J. Energy Res.* **2019**, *43*, 7790.
- (8) Sreenivasulu, B.; Sreedhar, I.; Suresh, P.; Raghavan, K. V. Development Trends in Porous Adsorbents for Carbon Capture. *Environ. Sci. Technol.* **2015**, *49*, 12641–12661.
- (9) MacDowell, N.; Florin, N.; Buchard, A.; Hallett, J.; Galindo, A.; Jackson, G.; Adjiman, C. S.; Williams, C. K.; Shah, N.; Fennell, P. An Overview of CO₂ Capture Technologies. *Energy Environ. Sci.* **2010**, *3*, 1645–1669.
- (10) Qian, Q.; Asinger, P. A.; Lee, M. J.; Han, G.; Mizrahi Rodriguez, K.; Lin, S.; Benedetti, F. M.; Wu, A. X.; Chi, W. S.; Smith, Z. P. MOF-Based Membranes for Gas Separations. *Chem. Rev.* **2020**, *120*, 8161.
- (11) Dutcher, B.; Fan, M.; Russell, A. G. Amine-Based CO₂ Capture Technology Development from the Beginning of 2013—A Review. *ACS Appl. Mater. Interfaces* **2015**, *7*, 2137–2148.
- (12) Zhao, B.; Su, Y.; Tao, W.; Li, L.; Peng, Y. Post-combustion CO₂ Capture by Aqueous Ammonia: A State-of-the-art Review. *Int. J. Greenhouse Gas Control* **2012**, *9*, 355–371.
- (13) Li, P.; Zeng, H. C. Hierarchical Nanocomposite by the Integration of Reduced Graphene Oxide and Amorphous Carbon with Ultrafine MgO Nanocrystallites for Enhanced CO₂ Capture. *Environ. Sci. Technol.* **2017**, *51*, 12998–13007.
- (14) Creamer, A. E.; Gao, B. Carbon-Based Adsorbents for Postcombustion CO₂ Capture: A Critical Review. *Environ. Sci. Technol.* **2016**, *50*, 7276–7289.
- (15) Wang, Q.; Luo, J.; Zhong, Z.; Borgna, A. CO₂ Capture by Solid Adsorbents and Their Applications: Current Status and New Trends. *Energy Environ. Sci.* **2011**, *4*, 42–55.
- (16) Askari, M.; Chung, T.-S. Natural Gas Purification and Olefin/Paraffin Separation Using Thermal Cross-Linkable Co-polyimide/ZIF-8 Mixed Matrix Membranes. *J. Membr. Sci.* **2013**, *444*, 173–183.
- (17) Japip, S.; Wang, H.; Xiao, Y.; Shung Chung, T. Highly Permeable Zeolitic Imidazolate Framework (ZIF)-71 Nano-particles Enhanced Polyimide Membranes for Gas Separation. *J. Membr. Sci.* **2014**, *467*, 162–174.
- (18) Liang, C. Z.; Liu, J. T.; Lai, J.-Y.; Chung, T.-S. High-Performance Multiple-layer PIM Composite Hollow Fiber Membranes for Gas Separation. *J. Membr. Sci.* **2018**, *563*, 93–106.
- (19) Japip, S.; Xiao, Y.; Chung, T.-S. Particle-Size Effects on Gas Transport Properties of 6FDA-Durene/ZIF-71 Mixed Matrix Membranes. *Ind. Eng. Chem. Res.* **2016**, *55*, 9507–9517.
- (20) He, S.; Jiang, X.; Li, S.; Ran, F.; Long, J.; Shao, L. Intermediate Thermal Manipulation of Polymers of Intrinsic Microporous (PIMs) Membranes for Gas Separations. *AIChE J.* **2020**, No. e16543.
- (21) Zhang, Y.; Cheng, X.; Jiang, X.; Urban, J. J.; Lau, C. H.; Liu, S.; Shao, L. Robust Natural Nanocomposites Realizing Unprecedented Ultrafast Precise Molecular Separations. *Mater. Today* **2020**, *36*, 40–47.
- (22) Jiang, X.; Li, S.; Shao, L. Pushing CO₂-philic Membrane Performance to the Limit by Designing Semi-interpenetrating Networks (SIPN) for Sustainable CO₂ Separations. *Energy Environ. Sci.* **2017**, *10*, 1339–1344.
- (23) Belmabkhout, Y.; Guillerm, V.; Eddaoudi, M. Low Concentration CO₂ Capture Using Physical Adsorbents: Are Metal–Organic Frameworks Becoming the New Benchmark Materials? *Chem. Eng. J.* **2016**, *296*, 386–397.
- (24) Long, J. R.; Yaghi, O. M. The Pervasive Chemistry of Metal–Organic Frameworks. *Chem. Soc. Rev.* **2009**, *38*, 1213–1214.
- (25) Li, H.; Eddaoudi, M.; Groy, T. L.; Yaghi, O. M. Establishing Microporosity in Open Metal–Organic Frameworks: Gas Sorption Isotherms for Zn(BDC) (BDC = 1,4-Benzenedicarboxylate). *J. Am. Chem. Soc.* **1998**, *120*, 8571–8572.
- (26) D'Alessandro, D. M.; Smit, B.; Long, J. R. Carbon Dioxide Capture: Prospects for New Materials. *Angew. Chem., Int. Ed.* **2010**, *49*, 6058–6082.
- (27) Ding, M.; Flraig, R. W.; Jiang, H.-L.; Yaghi, O. M. Carbon Capture and Conversion Using Metal–Organic Frameworks and MOF-Based Materials. *Chem. Soc. Rev.* **2019**, *48*, 2783–2828.
- (28) Hu, Z.; Wang, Y.; Shah, B. B.; Zhao, D. CO₂ Capture in Metal–Organic Framework Adsorbents: An Engineering Perspective. *Adv. Sustainable Syst.* **2019**, *3*, 1800080.

- (29) Burtch, N. C.; Jasuja, H.; Walton, K. S. Water Stability and Adsorption in Metal–Organic Frameworks. *Chem. Rev.* **2014**, *114*, 10575–10612.
- (30) Hong, D.-Y.; Hwang, Y. K.; Serre, C.; Férey, G.; Chang, J.-S. Porous Chromium Terephthalate MIL-101 with Coordinatively Unsaturated Sites: Surface Functionalization, Encapsulation, Sorption and Catalysis. *Adv. Funct. Mater.* **2009**, *19*, 1537–1552.
- (31) Bhattacharjee, S.; Chen, C.; Ahn, W.-S. Chromium Terephthalate Metal–Organic Framework MIL-101: Synthesis, Functionalization, and Applications for Adsorption and Catalysis. *RSC Adv.* **2014**, *4*, 52500–52525.
- (32) Férey, G.; Mellot-Draznieks, C.; Serre, C.; Millange, F.; Dutour, J.; Surblé, S.; Margiolaki, I. A Chromium Terephthalate-Based Solid with Unusually Large Pore Volumes and Surface Area. *Science* **2005**, *309*, 2040–2042.
- (33) Munusamy, K.; Sethia, G.; Patil, D. V.; Somayajulu Rallapalli, P. B.; Soman, R. S.; Bajaj, H. C. Sorption of Carbon Dioxide, Methane, Nitrogen and Carbon Monoxide on MIL-101(Cr): Volumetric Measurements and Dynamic Adsorption Studies. *Chem. Eng. J.* **2012**, *195–196*, 359–368.
- (34) Li, H.; Wang, K.; Feng, D.; Chen, Y.-P.; Verdegaal, W.; Zhou, H.-C. Incorporation of Alkylamine into Metal–Organic Frameworks through a Brønsted Acid–Base Reaction for CO₂ Capture. *ChemSusChem* **2016**, *9*, 2832–2840.
- (35) Zhou, Z.; Mei, L.; Ma, C.; Xu, F.; Xiao, J.; Xia, Q.; Li, Z. A Novel Bimetallic MIL-101(Cr, Mg) with High CO₂ Adsorption Capacity and CO₂/N₂ Selectivity. *Chem. Eng. Sci.* **2016**, *147*, 109–117.
- (36) Zhang, K.; Chen, Y.; Nalaparaju, A.; Jiang, J. Functionalized Metal–Organic Framework MIL-101 for CO₂ Capture: Multi-Scale Modeling from ab Initio Calculation and Molecular Simulation to Breakthrough Prediction. *CrystEngComm* **2013**, *15*, 10358–10366.
- (37) Emerson, A. J.; Chahine, A.; Batten, S. R.; Turner, D. R. Synthetic Approaches for the Incorporation of Free Amine Functionalities in Porous Coordination Polymers for Enhanced CO₂ Sorption. *Coord. Chem. Rev.* **2018**, *365*, 1–22.
- (38) Joshi, J. N.; Zhu, G.; Lee, J. J.; Carter, E. A.; Jones, C. W.; Lively, R. P.; Walton, K. S. Probing Metal–Organic Framework Design for Adsorptive Natural Gas Purification. *Langmuir* **2018**, *34*, 8443–8450.
- (39) Luan, Y.; Qi, Y.; Gao, H.; Andriamantsoa, R. S.; Zheng, N.; Wang, G. A General Post-Synthetic Modification Approach of Amino-Tagged Metal–Organic Frameworks to Access Efficient Catalysts for the Knoevenagel Condensation Reaction. *J. Mater. Chem. A* **2015**, *3*, 17320–17331.
- (40) Lee, Y.-R.; Yu, K.; Ravi, S.; Ahn, W.-S. Selective Adsorption of Rare Earth Elements over Functionalized Cr-MIL-101. *ACS Appl. Mater. Interfaces* **2018**, *10*, 23918–23927.
- (41) Wang, Z.; Cohen, S. M. Postsynthetic Covalent Modification of a Neutral Metal–Organic Framework. *J. Am. Chem. Soc.* **2007**, *129*, 12368–12369.
- (42) Yin, Z.; Wan, S.; Yang, J.; Kurmoo, M.; Zeng, M.-H. Recent Advances in Post-Synthetic Modification of Metal–Organic Frameworks: New Types and Tandem Reactions. *Coord. Chem. Rev.* **2019**, *378*, 500–512.
- (43) Bauer, S.; Serre, C.; Devic, T.; Horcajada, P.; Marrot, J.; Férey, G.; Stock, N. High-Throughput Assisted Rationalization of the Formation of Metal Organic Frameworks in the Iron(III) Amino-terephthalate Solvothermal System. *Inorg. Chem.* **2008**, *47*, 7568–7576.
- (44) Lin, Y.; Kong, C.; Chen, L. Direct Synthesis of Amine-Functionalized MIL-101(Cr) Nanoparticles and Application for CO₂ Capture. *RSC Adv.* **2012**, *2*, 6417–6419.
- (45) Jiang, D.; Keenan, L. L.; Burrows, A. D.; Edler, K. J. Synthesis and Post-Synthetic Modification of MIL-101(Cr)-NH₂ via A Tandem Diazotisation Process. *Chem. Commun.* **2012**, *48*, 12053–12055.
- (46) Han, G.; Qian, Q.; Mizrahi Rodriguez, K.; Smith, Z. P. Hydrothermal Synthesis of Sub-20 nm Amine-Functionalized MIL-101(Cr) Nanoparticles with High Surface Area and Enhanced CO₂ Uptake. *Ind. Eng. Chem. Res.* **2020**, *59*, 7888–7900.
- (47) Bromberg, L.; Diao, Y.; Wu, H.; Speakman, S. A.; Hatton, T. A. Chromium(III) Terephthalate Metal Organic Framework (MIL-101): HF-Free Synthesis, Structure, Polyoxometalate Composites, and Catalytic Properties. *Chem. Mater.* **2012**, *24*, 1664–1675.
- (48) Zhou, F.; Zhou, J.; Gao, X.; Kong, C.; Chen, L. Facile Synthesis of MOFs with Uncoordinated Carboxyl Groups for Selective CO₂ Capture via Postsynthetic Covalent Modification. *RSC Adv.* **2017**, *7*, 3713–3719.
- (49) Zhou, X.; Huang, W.; Miao, J.; Xia, Q.; Zhang, Z.; Wang, H.; Li, Z. Enhanced Separation Performance of A Novel Composite Material Gro@MIL-101 for CO₂/CH₄ Binary Mixture. *Chem. Eng. J.* **2015**, *266*, 339–344.
- (50) Chen, C.; Feng, N.; Guo, Q.; Li, Z.; Li, X.; Ding, J.; Wang, L.; Wan, H.; Guan, G. Template-Directed Fabrication of MIL-101(Cr)/Mesoporous Silica Composite: Layer-Packed Structure and Enhanced Performance for CO₂ Capture. *J. Colloid Interface Sci.* **2018**, *513*, 891–902.
- (51) Kayal, S.; Chakraborty, A. Impact of Alkali-Metal Impregnation on MIL-101 (Cr) Metal–Organic Frameworks for CH₄ and CO₂ Adsorption Studies. *ChemPhysChem* **2018**, *19*, 3158–3165.
- (52) McDonald, T. M.; D'Alessandro, D. M.; Krishna, R.; Long, J. R. Enhanced Carbon Dioxide Capture upon Incorporation of N,N'-Dimethylethylenediamine in the Metal–Organic Framework CuBT-Tri. *Chem. Sci.* **2011**, *2*, 2022–2028.
- (53) Vilela, S.; Salcedo-Abraira, P.; Colinet, I.; Salles, F.; de Koning, M.; Serre, C.; Horcajada, P. Nanometric MIL-125-NH₂ Metal–Organic Framework as A Potential Nerve Agent Antidote Carrier. *Nanomaterials* **2017**, *7*, 321.
- (54) Schaate, A.; Roy, P.; Godt, A.; Lippke, J.; Waltz, F.; Wiebcke, M.; Behrens, P. Modulated Synthesis of Zr-Based Metal-Organic Frameworks: From Nano to Single Crystals. *Chem. - Eur. J.* **2011**, *17*, 6643–6651.
- (55) Jiang, D.; Burrows, A. D.; Edler, K. J. Size-controlled Synthesis of MIL-101(Cr) Nanoparticles with Enhanced Selectivity for CO₂ over N₂. *CrystEngComm* **2011**, *13*, 6916–6919.
- (56) Hu, T.; Lv, H.; Shan, S.; Jia, Q.; Su, H.; Tian, N.; He, S. Porous Structured MIL-101 Synthesized with Different Mineralizers for Adsorptive Removal of Oxytetracycline from Aqueous Solution. *RSC Adv.* **2016**, *6*, 73741–73747.
- (57) Patterson, A. L. The Scherrer Formula for X-Ray Particle Size Determination. *Phys. Rev.* **1939**, *56*, 978–82.
- (58) Hu, Z.; Castano, I.; Wang, S.; Wang, Y.; Peng, Y.; Qian, Y.; Chi, C.; Wang, X.; Zhao, D. Modulator Effects on the Water-Based Synthesis of Zr/Hf Metal-Organic Frameworks: Quantitative Relationship Studies between Modulator, Synthetic Condition, and Performance. *Cryst. Growth Des.* **2016**, *16*, 2295–2301.
- (59) Zhao, T.; Jeremias, F.; Boldog, I.; Nguyen, B.; Henninger, S. K.; Janiak, C. High-Yield, Fluoride-Free and Large-Scale Synthesis of MIL-101(Cr). *Dalton Trans.* **2015**, *44*, 16791–16801.
- (60) Li, X.; Mao, Y.; Leng, K.; Ye, G.; Sun, Y.; Xu, W. Synthesis of Amino-Functionalized MIL-101(Cr) with Large Surface Area. *Mater. Lett.* **2017**, *197*, 192–195.
- (61) Côté, A. P.; Benin, A. I.; Ockwig, N. W.; ÓKeefe, M.; Matzger, A. J.; Yaghi, O. M. Porous, Crystalline, Covalent Organic Frameworks. *Science* **2005**, *310*, 1166–1170.
- (62) Kim, E. J.; Siegelman, R. L.; Jiang, H. Z. H.; Forse, A. C.; Lee, J. H.; Martell, J. D.; Milner, P. J.; Falkowski, J. M.; Neaton, J. B.; Reimer, J. A.; Weston, S. C.; Long, J. R. Cooperative Carbon Capture and Steam Regeneration with Tetraamine-Appended Metal–Organic Frameworks. *Science* **2020**, *369*, 392–396.
- (63) Mason, J. A.; Sumida, K.; Herm, Z. R.; Krishna, R.; Long, J. R. Evaluating Metal–Organic Frameworks for Post-Combustion Carbon Dioxide Capture via Temperature Swing Adsorption. *Energy Environ. Sci.* **2011**, *4*, 3030–3040.
- (64) Burtch, N. C.; Jasuja, H.; Dubbeldam, D.; Walton, K. S. Molecular-level Insight into Unusual Low Pressure CO₂ Affinity in

- Pillared Metal–Organic Frameworks. *J. Am. Chem. Soc.* **2013**, *135*, 7172–7180.
- (65) Li, R.; Ren, X.; Feng, X.; Li, X.; Hu, C.; Wang, B. A highly Stable Metal- and Nitrogen-Doped Nanocomposite Derived from Zn/Ni-ZIF-8 Capable of CO₂ Capture and Separation. *Chem. Commun.* **2014**, *50*, 6894–6897.
- (66) Shi, Z.; Tao, Y.; Wu, J.; Zhang, C.; He, H.; Long, L.; Lee, Y.; Li, T.; Zhang, Y.-B. Robust Metal–Triazolate Frameworks for CO₂ Capture from Flue Gas. *J. Am. Chem. Soc.* **2020**, *142*, 2750–2754.
- (67) Chen, C.-X.; Wei, Z.; Jiang, J.-J.; Fan, Y.-Z.; Zheng, S.-P.; Cao, C.-C.; Li, Y.-H.; Fenske, D.; Su, C.-Y. Precise Modulation of the Breathing Behavior and Pore Surface in Zr-MOFs by Reversible Post-Synthetic Variable-Spacer Installation to Fine-Tune the Expansion Magnitude and Sorption Properties. *Angew. Chem., Int. Ed.* **2016**, *55*, 9932–9936.
- (68) Hu, Z.; Faucher, S.; Zhuo, Y.; Sun, Y.; Wang, S.; Zhao, D. Combination of Optimization and Metalated-Ligand Exchange: An Effective Approach to Functionalize UiO-66(Zr) MOFs for CO₂ Separation. *Chem.—Eur. J.* **2015**, *21*, 17246–17255.
- (69) Vaidhyanathan, R.; Iremonger, S. S.; Shimizu, G. K. H.; Boyd, P. G.; Alavi, S.; Woo, T. K. Competition and Cooperativity in Carbon Dioxide Sorption by Amine-Functionalized Metal-Organic Frameworks. *Angew. Chem., Int. Ed.* **2012**, *51*, 1826–1829.
- (70) Caskey, S. R.; Wong-Foy, A. G.; Matzger, A. J. Dramatic Tuning of Carbon Dioxide Uptake via Metal Substitution in a Coordination Polymer with Cylindrical Pores. *J. Am. Chem. Soc.* **2008**, *130*, 10870–10871.
- (71) Vaidhyanathan, R.; Iremonger, S. S.; Dawson, K. W.; Shimizu, G. K. H. An Amine-Functionalized Metal Organic Framework for Preferential CO₂ Adsorption at Low Pressures. *Chem. Commun.* **2009**, *35*, 5230–5232.
- (72) Lin, Y.; Kong, C.; Chen, L. Amine-Functionalized Metal–Organic Frameworks: Structure, Synthesis and Applications. *RSC Adv.* **2016**, *6*, 32598–32614.
- (73) Khutia, A.; Janiak, C. Programming MIL-101Cr for Selective and Enhanced CO₂ Adsorption at Low Pressure by Postsynthetic Amine Functionalization. *Dalton Trans.* **2014**, *43*, 1338–1347.
- (74) Chen, C.; Feng, N.; Guo, Q.; Li, Z.; Li, X.; Ding, J.; Wang, L.; Wan, H.; Guan, G. Surface Engineering of A Chromium Metal–Organic Framework with Bifunctional Ionic Liquids for Selective CO₂ Adsorption: Synergistic Effect Between Multiple Active Sites. *J. Colloid Interface Sci.* **2018**, *521*, 91–101.
- (75) Lin, Y.; Yan, Q.; Kong, C.; Chen, L. Polyethyleneimine Incorporated Metal–Organic Frameworks Adsorbent for Highly Selective CO₂ Capture. *Sci. Rep.* **2013**, *3*, 1859.
- (76) Llewellyn, P. L.; Bourrelly, S.; Serre, C.; Vimont, A.; Daturi, M.; Hamon, L.; De Weirerd, G.; Chang, J.-S.; Hong, D.-Y.; Kyu Hwang, Y.; Hwa Jhung, S.; Férey, G. High Uptakes of CO₂ and CH₄ in Mesoporous Metal–Organic Frameworks MIL-100 and MIL-101. *Langmuir* **2008**, *24*, 7245–7250.
- (77) Liu, Q.; Ning, L.; Zheng, S.; Tao, M.; Shi, Y.; He, Y. Adsorption of Carbon Dioxide by MIL-101(Cr): Regeneration Conditions and Influence of Flue Gas Contaminants. *Sci. Rep.* **2013**, *3*, 2916.
- (78) Wang, Q. M.; Shen, D. M.; Bulow, M.; Lau, M. L.; Deng, S. G.; Fitch, F. R.; Lemcoff, N. O.; Semanscin, J. Metallo-Organic Molecular Sieve for Gas Separation and Purification. *Microporous Mesoporous Mater.* **2002**, *55*, 217–230.
- (79) Millward, A. R.; Yaghi, O. M. Metal–Organic Frameworks with Exceptionally High Capacity for Storage of Carbon Dioxide at Room Temperature. *J. Am. Chem. Soc.* **2005**, *127*, 17998–17999.
- (80) Couck, S.; Denayer, J. F. M.; Baron, G. V.; Rémy, T.; Gascon, J.; Kapteijn, F. An Amine-Functionalized MIL-53 Metal–Organic Framework with Large Separation Power for CO₂ and CH₄. *J. Am. Chem. Soc.* **2009**, *131*, 6326–6327.
- (81) Kim, S.-N.; Kim, J.; Kim, H.-Y.; Cho, H.-Y.; Ahn, W.-S. Adsorption/Catalytic Properties of MIL-125 and NH₂-MIL-125. *Catal. Today* **2013**, *204*, 85–93.
- (82) Park, Y.; Moon, D.-K.; Kim, Y.-H.; Ahn, H.; Lee, C.-H. Adsorption Isotherms of CO₂, CO, N₂, CH₄, Ar and H₂ on Activated Carbon and Zeolite LiX up to 1.0 MPa. *Adsorption* **2014**, *20*, 631–647.